

# Novel Hyperspectral Prediction Method and Apparatus

Gabor J Kemeny, Natalie A Crothers, Gard A Groth and Kathy A Speck, Middleton Research, Middleton WI 53562

Ralf Marbach, VTT Optical Instruments Centre, Oulu FIN-90571, Finland

## ABSTRACT

Both the power and the challenge of hyperspectral technologies is the very large amount of data produced by spectral cameras. While off-line methodologies allow the collection of gigabytes of data, extended data analysis sessions are required to convert the data into useful information. In contrast, real-time monitoring, such as on-line process control, requires that compression of spectral data and analysis occur at a sustained full camera data rate. Efficient, high-speed practical methods for calibration and prediction are therefore sought to optimize the value of hyperspectral imaging.

A novel method of matched filtering known as science based multivariate calibration (SBC) was developed for hyperspectral calibration. Classical (MLR) and inverse (PLS, PCR) methods are combined by spectroscopically measuring the spectral “signal” and by statistically estimating the spectral “noise.” The accuracy of the inverse model is thus combined with the easy interpretability of the classical model. The SBC method is optimized for hyperspectral data in the Hyper-Cal™ software used for the present work. The prediction algorithms can then be downloaded into a dedicated FPGA based High-Speed Prediction Engine™ module. Spectral pretreatments and calibration coefficients are stored on interchangeable SD memory cards, and predicted compositions are produced on a USB interface at real-time camera output rates. Applications include minerals, pharmaceuticals, food processing and remote sensing.

## INTRODUCTION

Hyperspectral imaging is the science of creating spatial information using the spectra of each point in the measured scene. In the laboratory setting, samples such as pharmaceutical formulations with blending profiles and complex physical structures need to be tested. In process monitoring, pull samples and single point monitoring are often not sufficient to assure uniformity of products that are blended, coated or dried. In homeland security applications, the entire surface of objects, such as packages, need to be monitored, with materials detected in the full scene, not just a single point or direction. All of these applications benefit from hyperspectral imaging (HSI). When the purpose of the imaging is the measurement of the concentration of ingredients or the chemical recognition of materials, the technique is called chemical imaging (CI).

Hyperspectral imaging can be performed in UV, visible, near- far-and mid-infrared. This paper addresses the near-infrared spectral region from 1000 nm to 2500 nm, where most materials have a unique spectral profile and where the light penetration and reflectance allows good quality *in situ* measurements without requiring material dilution. Chemical imaging in the near-infrared for pharmaceutical applications was reviewed by Koehler et al.<sup>1</sup>, and its advantages for the FDA’s process analytical technologies initiative (PAT) described by Lewis et al.<sup>2</sup>.

A new method for multivariate calibration of spectroscopic data was developed<sup>3,4,5</sup>. The method, originally referred to as “Specific Wiener Filter,” but later re-named Science-Based Calibration (SBC) by industry practitioners, recognizes the fact that multivariate calibration, as a technical discipline, is part of the field of time signal processing, rather than statistics. This change in the point of view, combined with some added mathematics, shows the optimal chemometric solution to be nothing other than a spectral form of matched filter (in Europe, better known as Wiener filter). Secondly and more importantly, simple ways to perform calibration in practice become apparent and available, often providing significant advantages over the current practice of statistical calibration (PLS, PCR). For complex applications, the time and cost of

multivariate calibration can be drastically reduced, often by 80%, while at the same time increasing the quality of the result.

The chemometric literature contains a series of papers on the net analyte signal (NAS), which is defined as that part of the pure component spectrum that is orthogonal to all other spectra<sup>6,7</sup>. The NAS is directly comparable to the orthogonal subspace projection approach proposed for hyperspectral image data processing by Harsanyi and Chang<sup>8</sup>. The chemometrics literature has subsequently shown that the NAS concept is incomplete and at times misleading<sup>9</sup>. The concept points in the right direction, i.e., tries to quantify how much of the pure component spectrum is useful in calibration, but it suffers from a basic insufficiency. In a thought experiment, the more spectra are included in the list of "other spectra," the smaller the NAS will be, even if the spectra included have very small amplitudes. The severeness of spectral overlap is obviously governed by both the spectral shape and the magnitude of the interfering component, so NAS is incomplete. Also, as first pointed out by Kailey and Illing<sup>10</sup>, the NAS solution was proven<sup>11</sup> to be identical to what is called "classical modeling" in chemometrics. The latter is known to be inferior to other methods, especially in complex situations where severe spectral overlap exists. In other words, the NAS known as orthogonal projection solution can in practice be inferior to the optimal solution which, in hyperspectral imaging as in other technical disciplines, is defined by the "matched" filter. The SBC method is a combination of the best features of the earlier "classical" and "inverse" approaches to multivariate calibration. The result is fully science-based *and* optimal in the mean-square error sense, i.e., measurement accuracy is as good or better than the results from costly statistical calibration. Below, are a few examples of matched filtering in SWIR hyperspectral imaging.

## EXPERIMENTAL

For the measurements, SWIR-LVDS-100-N25E hyperspectral cameras (Spectral Imaging Ltd. (Specim), Oulu, Finland) with four-stage thermoelectrically cooled Mercury-Cadmium-Telluride (MCT) focal plane array detectors were used. The sensor in the camera contained 320 spatial and 256 spectral pixels, and covered the 970-2500 nm wavelength range. The camera worked on the push-broom principle, providing a 15-30 times better throughput than similar acousto-optic tunable filter (AOTF) or liquid crystal tunable filter (LCTF) based cameras<sup>12</sup>.

For the laboratory experiments, a SisuCHEMA™ hyperspectral system (Specim) was used. The system consists of the above mentioned SWIR camera, a line illumination system and a computer controlled sampling stage. For the larger samples, the same SWIR camera was equipped with a fixed 15 mm hyperspectral flat field near-infrared lens, optimized for the 970-2500 nm region. Small samples, less than 10 mm wide, were measured with a 1:1 imaging lens, providing approximately 30 μm resolution.

For the outdoor experiments, a wide angle MSCR/SWIR mirror scanner with serial interface was added (Specim). The scan angle was typically adjusted to approximately 90 degrees to capture a wide scene. The camera was mounted on a tripod, which may also be used to mount and direct additional cameras, such as visible range (400-800 nm) or VNIR cameras (400-1000 nm), to the same sample, or same scene.

Mineral samples were identified by a recognized mineral expert, cut with a diamond saw and measured with the raw cut, unpolished side facing the camera.

Pharmaceutical model mixtures were prepared gravimetrically with an analytical balance, thoroughly mixed and placed in separate cups of a plastic tray without adjusting or smoothing the top surface of the blends. Lactose, cellulose and magnesium stearate were obtained from Sigma-Aldrich (Milwaukee, WI).

Outdoor scans were performed on a cold, sunny day using the ambient light as illumination. A small patch of talc (Sigma-Aldrich) was spilled on the pavement in a thin layer and measured from a distance of approximately 40 feet.

Measurement time in all cases was under 5 seconds, integration time 3-10 msec and the camera speed 50-100 frames per second.

Pure analyte reference spectra were obtained on an Antaris™ FT-NIR spectrometer (ThermoFisher Scientific, Waltham, MA) in reflectance, using an integrating sphere sampling arrangement. Spectra were obtained using an optical resolution close to that of the SWIR camera (approx. 32 cm<sup>-1</sup>) or extracted from the image of the pure material.

## THEORY

In the following, we assume full hyperspectral data ( $x, y, \lambda$ ) to be available, i.e., we assume that a fully resolved spectrum is measured at each spatial pixel's location. For brevity of discussion, we focus on the spectral dimension ( $\lambda$ ) in the following, and omit the spatial variables ( $x, y$ ) in the equations. In other words, the following discussion and equations consider "one pixel at a time."

The basic assumption behind any spectrometry is that the measured spectrum contains a response from the analyte of interest:

$$\mathbf{x}^T = y \cdot \mathbf{g}^T + \mathbf{x}_n^T \quad [\text{AU}] \quad (1)$$

where vector  $\mathbf{x}^T$  the measured spectrum at the given pixel (in units of e.g. absorbance "units," [AU]); scalar  $y$  the true (and sought-after) concentration of the analyte of interest at the given pixel (in units of, say, [weight%]);  $\mathbf{g}^T$  the response spectrum of the analyte of interest [AU/(weight%)]; and  $\mathbf{x}_n^T$  [AU] is everything in the measured spectrum that is *not* from the analyte of interest, including instrumental noise *and* interfering spectra.

The shape of the response spectrum of the analyte of interest,  $\mathbf{g}^T$ , is determined not only by the chemical structure and state of the sample, but usually also by its physical properties (e.g. scattering) and the type of sampling optics.

The spectral signal is described by a mean,  $\bar{y} \cdot \mathbf{g}^T$ , and a root-mean-square (RMS),  $\sigma_y \cdot \mathbf{g}^T$ , where  $\sigma_y$  is the standard deviation of  $y$ . Likewise, the spectral noise is described by a mean,  $\bar{\mathbf{x}}_n^T$ , and a covariance matrix,  $\Sigma$ . The latter can be estimated as follows: assume for a moment that a large number, say 10,000, NIR spectra can be measured, for example from pharmaceutical tablets with *constant* concentration of the active ingredient, say, 200 mg. In other words, the differences between these spectra are solely due to variations in the other constituents and noise sources. Writing all these spectra into one matrix,  $\mathbf{X}$ ,

$$\mathbf{X} = \begin{pmatrix} \mathbf{x}_1^T \\ \mathbf{x}_2^T \\ \vdots \\ \mathbf{x}_{10,000}^T \end{pmatrix} = \begin{pmatrix} 200 \text{ mg} \\ 200 \text{ mg} \\ \vdots \\ 200 \text{ mg} \end{pmatrix} \cdot \mathbf{g}^T + \begin{pmatrix} \mathbf{x}_{n,1}^T \\ \mathbf{x}_{n,2}^T \\ \vdots \\ \mathbf{x}_{n,10,000}^T \end{pmatrix} = y \cdot \mathbf{g}^T + \mathbf{X}_n \quad (2)$$

shows that after mean-centering, the measured spectra represent only spectral noise,

$$\tilde{\mathbf{X}} = \tilde{\mathbf{X}}_n \quad (3)$$

where the "~" tilde means that the matrix is mean-centered (the average row is subtracted from all the rows). Thus, the covariance matrix of the spectral noise can be estimated as,

$$\Sigma \cong \frac{\tilde{\mathbf{X}}^T \tilde{\mathbf{X}}}{10,000 - 1} \quad [\text{AU}^2] \quad (4)$$

If the NIR spectra contain, e.g., 256 spectral variables (wavelengths), then matrix  $\tilde{\mathbf{X}}$  has dimension 10,000 rows x 256 columns, and matrix  $\mathbf{\Sigma}$  has dimension 256 x 256.

It turns out that the optimum solution to the measurement problem, Eq.(1), is a function of the quantities introduced above. The optimum  $b$ -vector in the minimum mean-square prediction error sense is [1],

$$\mathbf{b}_{opt} = \frac{\sigma_y^2 \mathbf{\Sigma}^- \mathbf{g}}{1 + \sigma_y^2 \mathbf{g}^T \mathbf{\Sigma}^- \mathbf{g}} \quad [\text{mg / AU}] \quad (5)$$

where  $\mathbf{\Sigma}^-$  the inverse of  $\mathbf{\Sigma}$ . The "1" in the denominator of Eq.(5) is responsible for the familiar effect that the slope in the prediction scatter plot turns down towards zero if the "range,"  $\sigma_y$ , of the calibration signal is too small. If the "range" is large ( $\sigma_y^2 \rightarrow \infty$ ), then Eq.(5) turns towards,

$$\mathbf{b}_{opt(1)} = \frac{\mathbf{\Sigma}^- \mathbf{g}}{\mathbf{g}^T \mathbf{\Sigma}^- \mathbf{g}} \quad (6)$$

which is the desired, unity-slope result. When  $\mathbf{b}_{opt(1)}$  is used to predict the concentration value of a new spectrum,  $\mathbf{x}_{pred}^T$ ,

$$y_{pred} = \bar{y} + (\mathbf{x}_{pred} - \bar{\mathbf{x}})^T \cdot \mathbf{b}_{opt(1)} \quad [\text{mg}] \quad (7)$$

(where  $\bar{\mathbf{x}}^T = \bar{y} \cdot \mathbf{g}^T + \bar{\mathbf{x}}_n^T$ ) then the standard error of prediction *a.k.a.* standard deviation of  $(y_{pred} - y)$  is,

$$SEP_{opt} = \sqrt{\frac{1}{\mathbf{g}^T \cdot \mathbf{\Sigma}^- \cdot \mathbf{g}}} \quad [\text{mg}_{\text{RMS}}] \quad (8)$$

Equation (8) is the spectroscopic, multivariate limit of detection of signal  $\mathbf{g}$  in noise  $\mathbf{\Sigma}$ . In other words, Eq.(8) is the *sensitivity* limit. (The second limit of multivariate detection, *specificity*, can also be strictly defined, compare with the discussion in ref.4.) When validating the spectroscopic method, Eq.(6), against a lab-reference method, the prediction "error" measured (e.g. in the usual PRESS<sup>1/2</sup> statistic) is Eq.(8) *plus* the inaccuracy of the lab method itself.

The PRESS<sup>1/2</sup> result of a PLS or PCR calibration can be shown<sup>3</sup> to converge with increasing number of calibration standards towards the value of Eq.(8) *if* the error of the lab-reference method is zero *and* the prediction slope is one *and* the unspecific correlations (compare with ref. 4) are zero.

To summarize, the matched-filtering also known as SBC method (in its basic form) involves the followings steps:

- (a) determine "manually" the response spectrum of the analyte of interest,  $\mathbf{g}$ , in units of, e.g., [AU/mg]; (similar to the "K-matrix" approach)
- (b) collect a representative population of "noise" spectra and compute  $\mathbf{\Sigma}$  using Eq.(4); (as in the "statistical" approach, but without the need for reference values)
- (c) compute  $\mathbf{b}_{opt(1)}$  using Eq.(6); and
- (d) predict new spectra using Eq.(7), where  $\bar{y}$  and  $\bar{\mathbf{x}}^T$  the mean analyte concentration and the mean spectrum of the "noise" spectra that were used for computing  $\mathbf{\Sigma}$ . (Note that in cases where mean-centering is not desired,  $\bar{y}$  and  $\bar{\mathbf{x}}^T$  are effectively defined as zero.)

## RESULTS

Different minerals, all of which are used in the jade trade as acknowledged or unacknowledged substitutes, were measured on an FTNIR instrument (Fig.1) and the diffuse reflectance spectra was used to predict the images obtained using the SWIR camera system. The particular set of stones were all very clearly identifiable in the near-infrared, making near-infrared a good technique to identify adulterated artifacts.

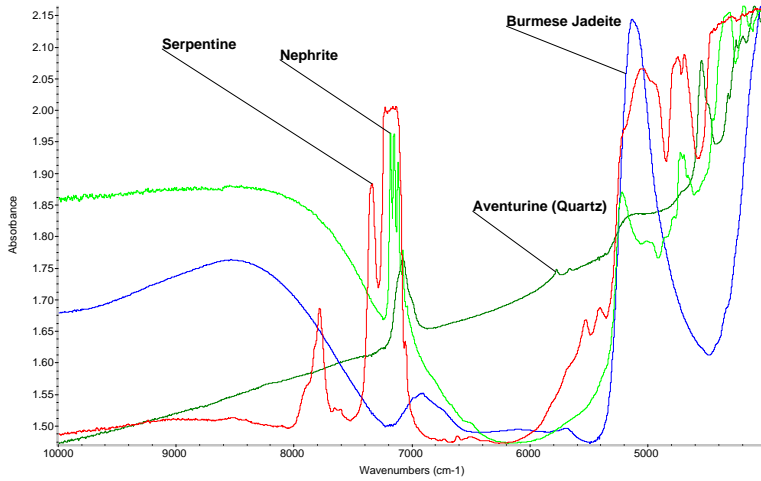


Fig 1. FT-NIR spectra of authentic jade and jade substitutes

A set of selected stones was arranged under the SWIR camera and scanned in the 100-2500 nm region. The normalized spectra were predicted using the pure components indicated below. The homogeneous jadeite on Fig 2a on the left (red on the color image or dark spot on the black&white image) was predicted uniformly, the nephrite mineral predicted the highest in the set, right lower corner on Fig 2b, but it apparently contained veins of other minerals with slightly different spectral characteristics and was predicted with a non-uniform pattern.

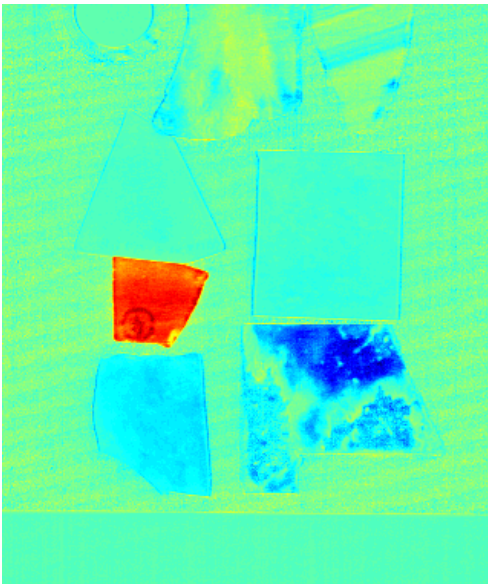


Fig 2a Prediction image using jadeite spectrum

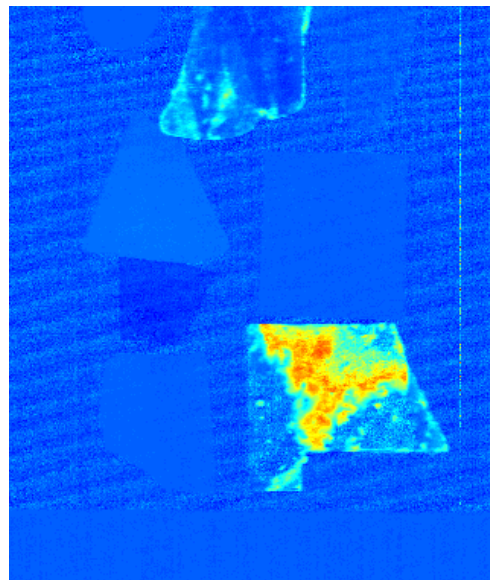


Fig 2b Prediction image of the same file using nephrite spectrum

In order to illustrate the quantitative prediction of the SBC technique in imaging, a model mixture of three pharmaceutical excipients was prepared. The concentration of the ingredients varied from 0-100%, which is usually a very demanding application in the near-infrared reflectance due to non-linearities. The results of the calibration were very good and even transferable to a laboratory FTNIR as reported<sup>13</sup>. The SBC prediction example shows on a color scale, lactose (center well in bottom row) at 100%, other wells according to their lactose composition. It is interesting to note that the surfaces of the wells are not reported as uniform, even though the composition is the same throughout the well. In conventional near-infrared measurement, the area would be averaged and differences would not show up. In imaging however surface unevenness as well as shadows from the rims of the wells, appear as small composition differences. In earlier examples, higher magnification of pure materials, similar to these excipients, the image of individual crystals of other materials in earlier experiments also show “concentration” differences due to changes in local scattering, specular and diffuse reflectance differences and micro-shadows between the crystals<sup>14</sup>.

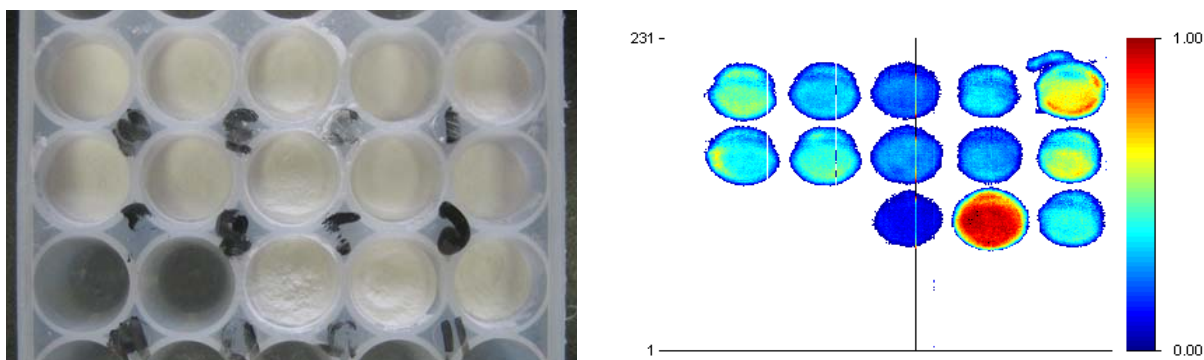


Fig 3. Ternary mixtures of lactose, Mg-stearate and cellulose in small plastic cups and SBC predicted image based on the pure ingredient spectra. Lactose concentrations (w/w%) from right to left: 88.0, 31.8, 29.2, 28.0, 50.6, 72.1, 33.5, 33.6, 41.2, 47.9. Bottom row: 0% (pure Mg-stearate), 100% (pure lactose), 0%(pure cellulose). Scale of predicted composition is ranging from blue (0%) to red (100%) not clearly discernible on the black and white image.

The prediction technique was also tested on a simple model, spilling a small amount of a known substance outdoors, as shown on the reference photo on the left. The camera was mounted at about a 40 feet distance scanning the same scene. The SBC prediction, calculated with the near infrared spectrum of talc, enhances the spot (which is red on the original plot, indicating higher concentration).

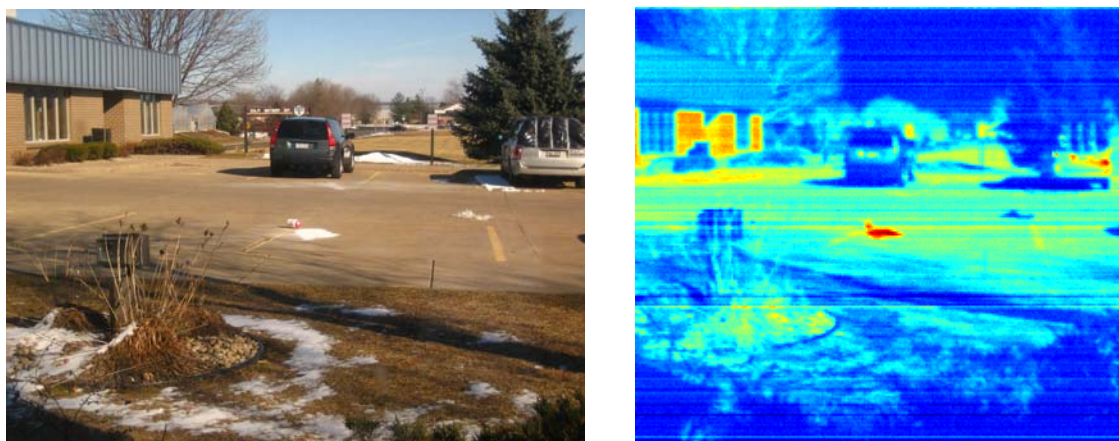


Fig.4 Image and SBC prediction of a powder spill

Outdoor scenes are very complex spectroscopically and quite different from spectra produced in the laboratory with a quartz halogen source. Therefore, in this case example, the spectrum had to be limited to one characteristic region of the powder, and some of the zones of the image had to be used to reduce the effects of overlapping spectral changes. This was accomplished<sup>11</sup> by adding the specific spectral shapes to the noise variance,  $\Sigma$ , to enhance the specificity of the prediction.

In addition to using the above techniques off-line, the prediction algorithms developed using SBC can be downloaded into a dedicated FPGA based High-Speed Prediction Engine™ module. The choice of spectral pretreatments and calibration coefficients are stored on interchangeable SD cards and the predicted compositions or parameters are produced on a USB interface, at the real-time camera output rate, for display or further machine vision evaluation. The combination of the SBC method with a high-speed prediction technology significantly enhances the capabilities and use of hyperspectral cameras.



Fig 5 Hyperspectral prediction module. Equations are downloaded into the module and composition prediction is achieved at the speed of the camera for each spatial point.

The authors are certain that practicing spectroscopists, statisticians, engineers and others involved in hyperspectral image analysis will appreciate the difficulties associated with establishing both the analyte response spectrum ( $g$ ), as it appears in the actual sample matrix and in the actual measurement set-up as the camera is seeing it, as well as estimating the noise ( $\Sigma$ ) in the images to be measured. Pure materials have different physical characteristics, particle size, crystallinity; depth of light penetration may be drastically different in the lab compared to that of a product or in a scene. Illumination may be different in angle and spectral content and reference spectrometers may have different resolution, signal-to-noise as well as a slightly different wavelength scale from the cameras. All of these factors must be considered by the expert applying the technique. It is also worth mentioning that not all imaging problems have a “pure” material assigned for the analyte of interest. In many cases, a spectral change or a spectroscopically unqualified feature must be explored and thus PCA or other methods must be used to characterize the sample. In spite of these obstacles, the technique is simple, fast and powerful, and certain to find its place among other, currently used hyperspectral imaging methods.

## REFERENCES

- [1] Koehler, F.W, Kidder, L.H., Lewis, E.N.: “Near infrared spectroscopy: the practical chemical imaging solution”, *Spectroscopy Europe* **14**/3 pp12-19 (2002)
- [2] Lewis, E.N., Schoppelrei, J., Lee E.: “Near-infrared Chemical Imaging and the PAT Initiative”, *Spectroscopy* **19**(4), 26 (2004)
- [3] Marbach, R.: “On Wiener Filtering and the Physics Behind Statistical Modeling”, *J. Biomed. Optics* **7**, 130-147 (2002)
- [4] Marbach, R.: “New Method for Multivariate Calibration”, *J. Near Infrared Spectrosc.* **13**, 241-254 (2005)

- [5] Marbach, R.: "Methods to significantly reduce the calibration cost of multichannel measurement instruments", US Pat. No. 6,629, 041 B1, 30 Sep. 2003
- [6] Lorber, A.: "Error propagation and figures of merit for quantification by solving matrix equations", *Anal. Chem.* **58**, 1167–1172 (1986)
- [7] Lorber, A., Faaber, K., and Kowalski, B. R.: "Net analyte signal calculation in multivariate calibration", *Anal. Chem.* **69**, 1620–1626 (1997)
- [8] Harsanyi, J. C. and Chang, C. I.: "Hyperspectral image classification and dimensionality reduction: An orthogonal subspace projection approach", *IEEE Trans. Geosci. Remote Sens.* **32**, 779–784 (1994)
- [9] Brown, C.D.: "Discordance between net analyte signal theory and practical multivariate calibration", *Anal. Chem.*, **76**, 4364-4373 (2004)
- [10] Kailey, W. F. and Illing, L.: "Small target detection against vegetative backgrounds using hyperspectral imagery", 1997 Meeting of the IRIS Specialty Group on Passive Sensors, Vol. **1**, pp. 423–429 (1997)
- [11] Marbach, R.: "On the Specificity of Chemometric Calibrations", IFPAC 2007, Baltimore MD
- [12] Hyvarinen, T., Herrala, E., Jussila, J., "High Speed Hyperspectral Imaging", 13th International Conference on Near Infrared Spectroscopy, Umeå, Sweden, June 17-21, 2007
- [13] Kemeny, G., Fuchs, N.: "Calibration Transfer from a Laboratory Based FTNIR to a High-Speed Line-Camera", Eastern Analytical Symposium, Somerset NJ, 2008
- [14] Kemeny, G.: "Near-Infrared Hyperspectral Imaging: A Practical Spectroscopist's View", International Diffuse Reflectance Conference, Chambersburg PA, 2008